Observational Evidence for Relationships between the Degree of Aggregation of Deep Convection, Water Vapor, Surface Fluxes, and Radiation

ISABELLE TOBIN, SANDRINE BONY, AND REMY ROCA

Laboratoire de Meteorologie Dynamique, Institut Pierre Simon Laplace, CNRS, and University Pierre and Marie Curie, Paris, France

(Manuscript received 11 May 2011, in final form 12 April 2012)

ABSTRACT

Tropical deep convection exhibits complex organization over a wide range of scales. This study investigates the relationships between the spatial organization of deep convection and the large-scale atmospheric state. By using several satellite datasets and reanalyses, and by defining a simple diagnostic of convective aggregation, relationships between the degree of convective aggregation and the amount of water vapor, turbulent surface fluxes, and radiation are highlighted above tropical oceans. When deep convection is more aggregated, the middle and upper troposphere are drier in the convection-free environment, turbulent surface fluxes are enhanced, and the low-level and midlevel cloudiness is reduced in the environment. Humidity and cloudiness changes lead to a large increase in outgoing longwave radiation. Cloud changes also result in reduced reflected shortwave radiation. Owing to these opposing effects, the sensitivity of the radiative budget at the top of the atmosphere to convective aggregation turns out to be weak, but the distribution of radiative heating throughout the troposphere is affected. These results suggest that feedbacks between convective aggregation and the large-scale atmospheric state might influence large-scale dynamics and the transports of water and energy and, thus, play a role in the climate variability and change. These observational findings are qualitatively consistent with previous cloud-resolving model results, except for the effects on cloudiness and reflected shortwave radiation. The proposed methodology may be useful for assessing the representation of convective aggregation and its interaction with the large-scale atmospheric state in various numerical models.

1. Introduction

In the tropics, deep convection constitutes the primary mechanism through which water vapor and energy are transported vertically in the troposphere. It is also responsible for a large part of the cloudiness and precipitation. Because deep convective regions are moister and cloudier than dry, subsiding areas, the fractional area of the tropics covered by deep convection is critical for the mean tropical climate and its sensitivity (Pierrehumbert 1995; Larson et al. 1999). At first order, the convective area is related to the large-scale circulation (Raymond 1995; Lau et al. 1997; Bony et al. 1997; Yang et al. 2003). For a given large-scale circulation, however, an ''amount of convection'' can occur under a variety of organizations, more or less clumped, over a wide range of scales. This can develop as individual thunderstorm cells, with little or no apparent organization, or in the form of mesoscale convective systems (MCSs) such as squall lines (Houze 1977; Redelsperger 1997) and mesoscale complexes (Laing and Fritsch 1997). They can group into bigger clusters until forming superclusters (Nakazawa 1988; Mapes 1993) and planetary envelopes such as the Madden–Julian oscillation (MJO) (Madden and Julian 1994).

What role does the spatial organization of convection play in the interaction between convection and its environment and what are the implications of convective organization for the large-scale atmospheric state? In other words, for comparable large-scale forcings and a given amount of convection (i.e., for a given precipitation amount or convective heating over a domain), are two different states of convective organization equivalent regarding the mean climate state? If not, climate feedbacks might be associated with convective organization changes.

Several cloud resolving model (CRM) studies, using the idealized framework of radiative–convective equilibrium (i.e., without imposing any large-scale flow),

Corresponding author address: Isabelle Tobin, Laboratoire de Meteorologie Dynamique, 4 place Jussieu, Paris 75252, France.
E-mail: itlmd@lmd.jussieu.fr

DOI: 10.1175/JCLI-D-11-00258.1

TABLE 1. Brief description of the datasets used to conduct this study.

Name	Variable	Spatial resolution	Temporal sampling	Period	Reference
CLAUS	IR brightness temperature	0.5°	3 hourly	1983–2005	Hodges et al. (2000)
HOAPS	Surface rain	1°	Twice daily	1988–2005	Andersson et al. (2010)
	Precipitable water				
	Surface sensible heat flux				
	Surface latent heat flux				
	Sea surface temperature				
	10-m wind speed				
	Air–sea difference in humidity				
ERA-Interim	RH	0.75° 37 levels	6 hourly	1989–present	Simmons et al. 2007
	Vertical velocity	0.75° 37 levels	6 hourly	1989–present	
AIRS	RH	1°	Twice daily	2002–present	Aumann et al. 2003
OLR-NOAA	OLR	2.5°	Daily	1976–present	Liebmann and Smith 1996
CERES	OLR	5°	Daily	2000–04	http://ceres.larc.nasa.gov/
	Reflected shortwave				

have suggested a dependence of the mean atmospheric state on the convective organization at the synoptic scale. In particular, when deep convection is ''localized'' (Held et al. 1993), ''aggregated'' (Bretherton et al. 2005; Nolan et al. 2007; Khairoutdinov and Emanuel 2010), or ''organized into bands'' (Tompkins 2001), the large-scale atmosphere is found to be much drier than when convection is scattered. From these results, a mechanism for climate regulation has been proposed (Khairoutdinov and Emanuel 2010) whereby a warmer climate might favor convective aggregation, lead to a drier troposphere, experience an increase in the outgoing longwave radiation, and thus result in a negative feedback on surface temperature.

In light of these studies, two questions arise: Is there any observational evidence for the dependence of the climate state on convective aggregation, such as an anticorrelation between atmospheric humidity and convective aggregation? And is it possible to quantify this dependence? This latter question is critical to assessing the role that this dependence might actually play in climate. To address these questions, a statistical analysis of the degree of aggregation of convection along with its large-scale environmental characteristics is carried out over tropical oceans by using several satellite datasets and meteorological reanalyses.

The paper is organized as follows. Section 2 presents the data and the analysis framework used to conduct the study. In section 3, a method is proposed to quantify the degree of aggregation of deep convection. Relationships between the aggregation state of convection and the large-scale atmospheric state with regard to humidity and energy fluxes are presented in section 4. A summary and a discussion are given in section 5.

2. Data and analysis framework

a. Data

This analysis is based on several datasets, whose details regarding resolution and time period are summarized in Table 1.

(i) The 50-km brightness temperature (BT) dataset produced by the Cloud Archive User Service (CLAUS) is used to detect deep convective clouds. It consists of a long-time series of global thermal infrared window channel (10.5–12.5 μm) imagery of the earth (Hodges et al. 2000). It is derived from channel 2 (10 μm) of the level B3 thermal infrared radiances from the operational meteorological satellites (geostationary and polar orbiting) participating in the International Satellite Cloud Climatology Project (ISCCP). Note that the ISCCP level B3 imagery is produced by subsampling the raw full-resolution data (~5 km, every 30 min) to a spatial resolution of 30 km and a temporal resolution of 3 h.

(ii) The precipitation rate is derived from the HOAPS-3-C data product, which is the new version of the Hamburg Ocean Atmosphere Parameters and Fluxes from Satellite Dataset (Andersson et al. 2010). The HOAPS-3-C sea surface temperature (SST), precipitable water, surface latent and sensible fluxes, difference between sea surface saturation specific humidity, and near-surface specific humidity, and 10-m wind speed products are used to characterize environmental conditions. Except for the SST dataset, all variables are derived from the Special Sensor Microwave Imager (SSM/I) carried

on board Defense Meteorological Satellite Program (DMSP) satellites. The swath of this instrument is 1400 km. The SST is derived from the Rosenstiel School of Marine and Atmospheric Science (RSMAS)–National Oceanographic Data Center (NODC) Advanced Very High Resolution Radiometer (AVHRR) carried on board National Oceanic and Atmospheric Administration (NOAA) satellites, which provides twice-daily datasets. It is here averaged to a daily value. The swath width is 2800 km.

(iii) Relative humidity profiles are obtained from the European Centre for Medium-Range Weather Forecasts (ECMWF) Interim Re-Analysis (ERA-Interim) dataset (Simmons et al. 2007). Relative humidity derived from the Atmospheric Infrared Sounder (AIRS) on board the *Aqua* satellite (Aumann et al. 2003) is also used. The twice-daily values are averaged to a daily value. The swath width is 1650 km.

(iv) The vertical velocity from ERA-Interim reanalyses is used to characterize large-scale dynamics.

(v) Radiative fluxes at the top of the atmosphere (TOA) are derived from two datasets: the NOAA interpolated outgoing longwave radiation (Liebmann and Smith,1996) product for the longwave component and the Earth Radiation Budget Experiment (ERBE)-like Monthly Geographical Averages (ES-4) 5.0° nested regional daily total-sky product from the Cloud and Earth's Radiant Energy System (CERES) on board *Terra* for both longwave and shortwave components.

b. Compositing analysis

To examine the relationships between the aggregation state of convection and the mean climate state, several atmospheric variables (viz, precipitable water, relative humidity, turbulent surface fluxes, and radiative fluxes at the top of the atmosphere) are composited by the degree of aggregation of convection (whose computation is presented in the next section). The study is conducted above the Pacific, Atlantic, and Indian Oceans, over a 17-yr time period (January 1989–December 2005) except when using CERES data (2000–04) or AIRS (2002–05). The analysis is carried out as follows:

At the synoptic scale—Here, the study is conducted over domains of $10° \times 10°$ (about 1100 km $\times$ 1100 km in the tropics) (Fig. 1), which are comparable to the domain sizes used in the CRM studies mentioned in the introduction. The degree of aggregation of convection is thus determined relative to these domains and the atmospheric variables are averaged over the domains. The $10° \times 10°$ domains are taken each 5° in latitude and 5° in longitude. Note that, within half a day, when only one SSM/I instrument operates, the entire tropical oceanic region cannot be scanned completely. The $10° \times 10°$ domains for which the number of missing values exceeds 15% are not included in the statistics in order to ensure that the large-scale state is properly sampled. The results are not sensitive to this threshold (checked down to 3%).

At the instantaneous scale—Only instantaneous data are used, except for OLR-NOAA, CERES, and AIRS, which are at a daily resolution. Since the time sampling differs between the datasets, the coincidence between the datasets is achieved with a maximal lag of 3 h (except for daily datasets).

The compositing analyses are carried out for a given amount of convective activity within the domain so as to interpret differences in the mean state as related to the aggregation state rather than as a consequence of the convective activity difference itself. Several proxies may be employed to characterize convective activity. The proxy used here is the domain-averaged instantaneous precipitation rate (Fig. 1). Different precipitation regimes are considered by binning the instantaneous precipitation rate (the bins are 1 or 3 mm day^{-1} wide; both bin sizes lead to similar results but the results with the widest bins are less noisy). Moreover, to ensure as much as possible that the relationships are not driven by differing large-scale forcings, aggregation composites are computed for given sea surface temperature (SST) and large-scale dynamical conditions. The width of the SST bins is 1°C. Each precipitation regime is associated with a distribution of vertical velocity at each vertical level. For each precipitation regime, aggregation composites are computed from situations having a comparable domain-averaged vertical velocity at 800, 500, and 300 hPa (this is ensured by selecting situations for which vertical velocity values are around the most likely values of the distributions, $\pm$20 hPa).

3. A diagnostic of the degree of aggregation of deep convection

The notion of aggregation is a way, among others, of characterizing the various forms of convective organization revealed by satellite imagery, ranging from randomly scattered convection to clumped, coherent clusters. However, given the complexity and the diversity of the

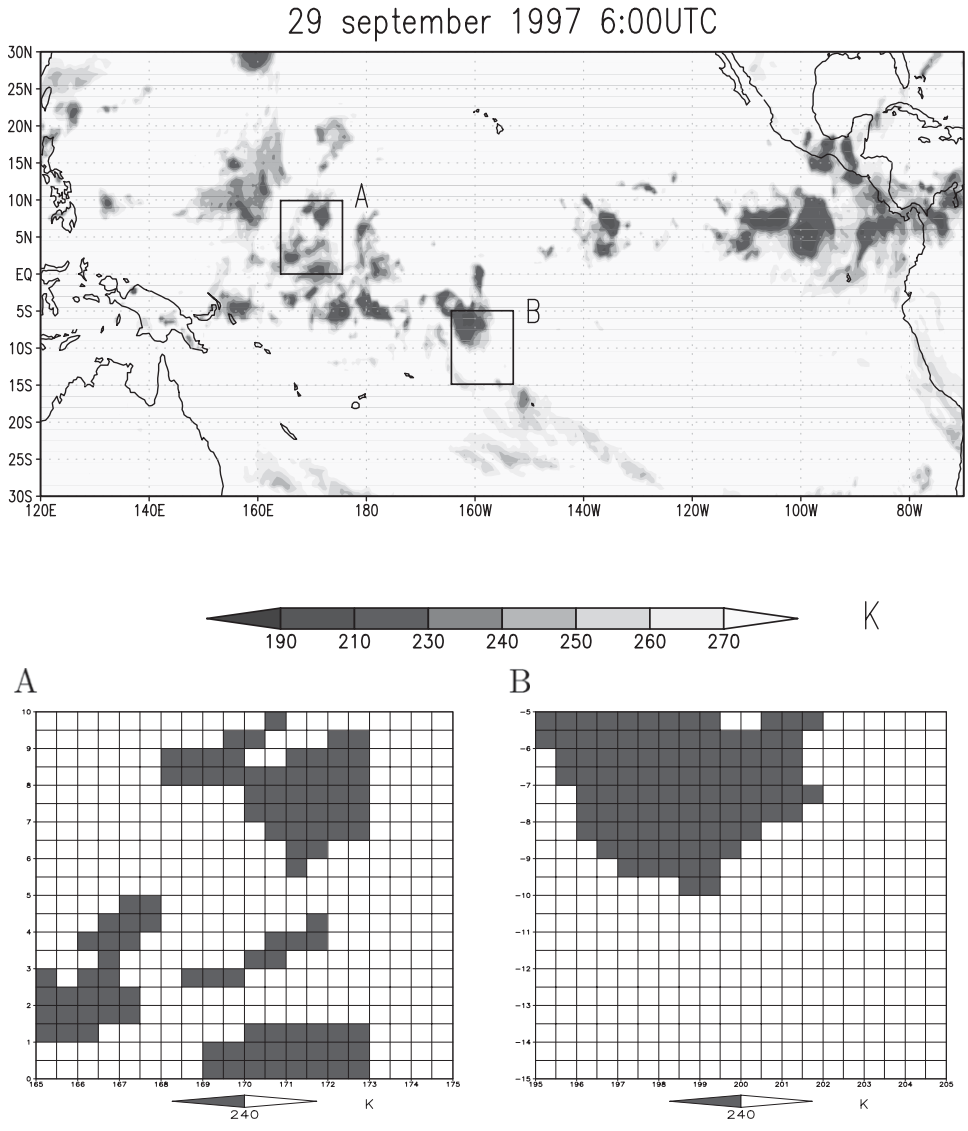

FIG. 1. (top) Snapshot of BT from CLAUS data at 0600 UTC 29 Sep 1997. The two black squares (A and B) are examples of the 10° × 10° domains under consideration in this study. (bottom) Segmentation of the domains into two parts: a deep convective region defined by the pixels with a BT colder than 240 K and the nonconvective environment (pixels warmer than 240 K). Both domains are characterized by the same domain-averaged rain rate (11 mm day^{-1}) but exhibit a different number of convective systems [A, six clusters; B, one cluster (using the four-connectivity clustering algorithm)].

convective organization at the synoptic scale, there is no univocally established nor unique definition for it. To capture different features of convective aggregation, several parameters are used here to measure the degree of convective aggregation, namely, the number of convective clusters within the domain under consideration, the clumping of these clusters over the domain, and a combination of both parameters. The method used in this study is kept simple and objective so as to be applied automatically to a large number of domains.

a. Aggregation parameters

The aggregation parameters are derived from CLAUS brightness temperature data (described in section 2). Consistently with many previous studies (Mapes and Houze 1993; Roca and Ramanathan 2000), pixels with a temperature below a certain threshold (here 240 K) are considered as being associated with the presence of deep convective systems. The convective threshold is chosen as warm compared to those in some

previous studies because the aim is not to spot convective cores but rather to identify convective systems (core plus anvil) or clusters as an entity. Pixels warmer than this threshold are referred to as the environment (Fig. 1). The coherent convective zones (or clusters) are identified with an algorithm of clustering, which consists of labeling adjacent nonzero pixels with a same index using four connectivity (i.e., two pixels belong to the same cluster only if they share a common side).

1) NUMBER OF CONVECTIVE CLUSTERS

For a given convective activity within a domain, the first parameter that appears to be relevant for characterizing the degree of convective aggregation is the number of convective clusters N within the domain (or, equivalently, the mean density of convective clusters over the domain). Viewed simply, the lower (larger) the number of clusters N, the more aggregated (scattered) the convection is. In Fig. 1 (bottom), the convection in scene A is less aggregated than that in scene B.

The wide range of N encountered in the observations (see Fig. 3a below) reflects the well-known variety of forms of convective organization. The probability density function (PDF) exhibits a dependence on precipitation regimes. The regimes of weak precipitation are associated with lower values of N. In stronger precipitation regimes, higher N are more frequent. However, the PDF becomes independent of the precipitation regime above about 9 mm day^{-1}, and exhibits a maximum for N around 2–3. The maximum N reached is about 13. Scenes with a unique cluster ($N = 1$) account for 15% of the observed cases. Situations with fewer than four clusters contribute to more than 50% of all cases and more than 90% of cases have a number smaller than seven. Situations with very numerous clusters within the domain are thus not frequently observed.

Note that the parameter N somewhat depends on the domain size, the spatial resolution of the brightness temperature data, and the temperature threshold used. But for the present study, the sorting of the convective scenes by the aggregation parameter matters more than the absolute values of these parameters. However, N can be normalized by a potential maximum of number Nmax, which is proportional to the ratio $(L/a)^2$, where L is the characteristic length of the domain and a is the size of the pixels (here, Nmax is equal to 200).

2) CLUMPING OF THE CLUSTERS

As shown by satellite imagery, an ensemble of N clusters is not necessarily uniformly distributed over the domain under consideration but can be more or less clumped (Figs. 2a,b). Therefore, when investigating the degrees of aggregation of convection, it is also relevant to consider an additional parameter aimed at characterizing the clumping of the clusters within the domain. Two measures of clumping of an ensemble of points are used in this study, namely, the so-called order-zero diameter D_0 and the Gini index (or order-one diameter) D_1 defined by Gauvrit and Delahaye (2006). For an ensemble of N points, they correspond, respectively, to the geometrical and arithmetical means of the distances d_i between points in pairs, respectively, $D_0 = \sqrt[n]{\prod_{i=1}^{n} d_i}$ and $D_1 = (1/n)\left(\sum_{i=1}^{n} d_i\right)$, where n is the number of pairs of clusters: $n = N(N-1)/2$. These measures are applied here to the centers of mass of the clusters. According to these definitions, short distances (or diameters) indicate the prevalence of clumped clusters within the domain (Fig. 2a) and the larger the distance, the more scattered the clusters are over the domain (Fig. 2b). Note that the range of $D_{0/1}$ values is dependent on the size of the domain considered. To find a parameter that characterizes clumping relative to a domain, the distances D_0 or D_1 are normalized by the characteristic length L (here, about 1000 km) of the domain under consideration. Note also that the finite size of the pixels sets a lower bound on the distances. Since the findings of the study are not affected by the choice of the distance (D_0 or D_1), only the analyses conducted with D_0 will be presented in this paper (after Fig. 3).

In Figs. 3c–f, the distributions of D_0 and D_1 (not normalized in this figure), sorted by domain-averaged precipitation regimes, show that for a given number of clusters N, the scattering of clusters over a $10° \times 10°$ domain is slightly increasing with precipitation. It can be explained by the tendency of the cluster size to increase with the domain-averaged precipitation rate. Weak precipitation regimes, however, favor the largest $D_{0/1}$ because the scattering of large clusters is limited by the finite size of the domain. Figure 4 shows that the mean D_0 of the clusters is independent of the number of clusters and the spread of the D_0 values rapidly decreases with N (Fig. 4). Indeed, when N is high, very short D_0 are not encountered because of the finite size of the clusters, whereas large D_0 are excluded by the limited size of the domain.

3) A COMBINED MEASURE OF N AND D_0: *SCAI*

Parameters N and D_0 are not equivalent [as shown by the distribution of pairs (D_0, N); Fig. 4] but provide a complementary way of characterizing the degree of aggregation of deep convection. To take into account both pieces of information, a third parameter is defined that is a simple combination of both parameters. It is referred to as the simple convective aggregation index (SCAI) and is the product of normalized N and D_0:

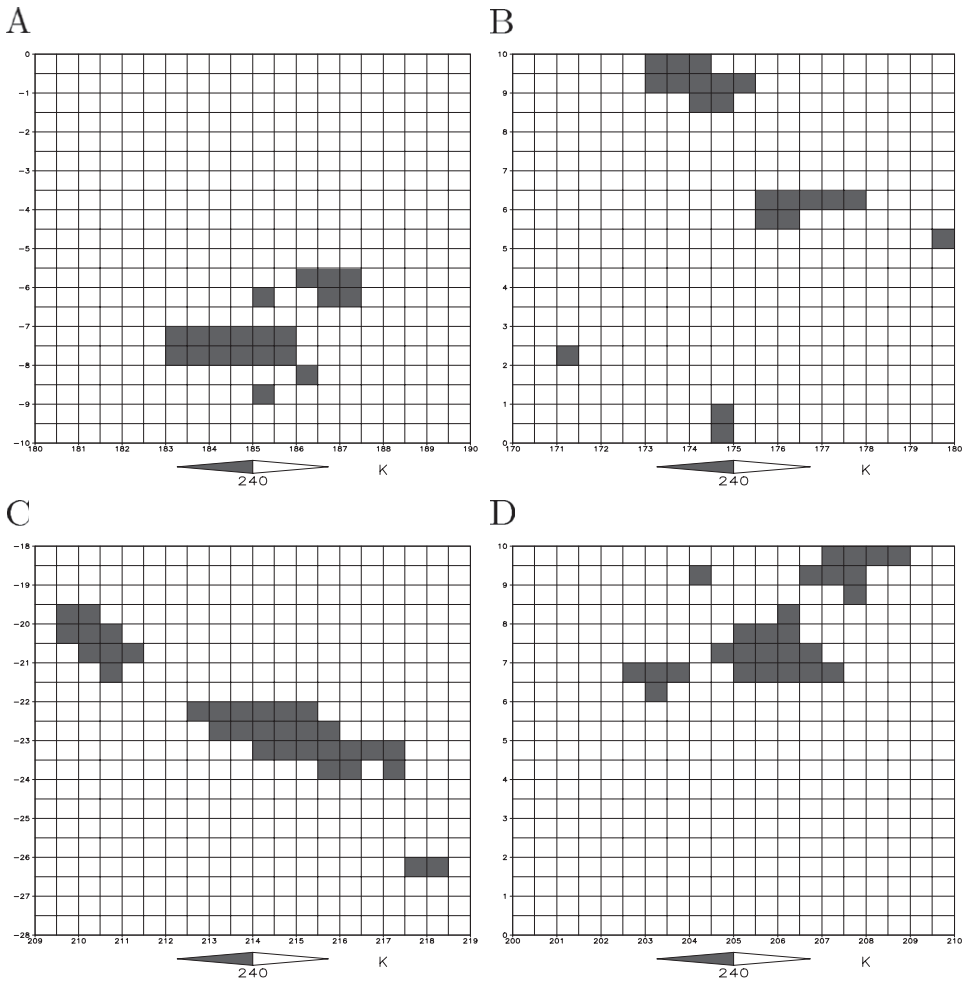

FIG. 2. Four examples of $10° \times 10°$ segmented domains: (a) 1200 UTC 11 Jul 1995, $N = 5$, $D_0 = 229$ km, $D_1 = 240$ km, SCAI = 5.73; (b) 1200 UTC 21 Jan 2003, $N = 5$, $D_0 = 668$ km, $D_1 = 720$ km, SCAI = 16.7; (c) 0600 UTC 21 Mar 1992, $N = 3$, $D_0 = 646$ km, $D_1 = 684$ km, SCAI = 9.7; and (d) 0000 UTC 11 Jan 1988, $N = 4$, $D_0 = 334$ km, $D_1 = 344$ km, and SCAI = 6.7.

$$\mathrm{SCAI} = \frac{N}{\mathrm{Nmax}} \frac{D_0}{L} \times 1000 = \tilde{N}\tilde{D}_0 \times 1000. \qquad (1)$$

This formula can be interpreted as the ratio of the degree of convective "disaggregation" to a potential maximal disaggregation, expressed in per thousand. For instance, in Fig. 2, SCAI will characterize scene A as being more aggregated than scene B and will consider scene D as more aggregated than scene C despite a higher number of clusters in D. Several combinations of N and D_0 have been tested. As they all lead to the same findings, as long as SCAI is an increasing function of both N and D_0, only one of them will be presented here. In cases where there is a unique cluster inside the domain, D_0 is set to zero. This choice leads to a discontinuity in D_0 values because of the finite size of the pixels, which leads to a break in the PDF of SCAI (Fig. 3b). As shown by the PDF of N, scenes with a unique cluster (SCAI equal to 0) account for 15% of all cases and 50% occur with an SCAI value lower than 6, whereas the encountered cases are spread over a range from 0 to roughly 30. The SCAI values lower than 13 (19) contribute to 80% (95%). Thus, like the PDFs of N and $D_{0/1}$, the PDF of SCAI shows that very scattered situations are not frequently observed.

b. *Preliminary characterization of the aggregation parameters*

To assess their ability to characterize the aggregation state of convection, the aggregation parameters are computed for two well-known extreme cases of aggregated convection, squall lines and tropical cyclones. Low values of aggregation parameters (computed over a chosen $10° \times 10°$ domain) characterize such cases. For

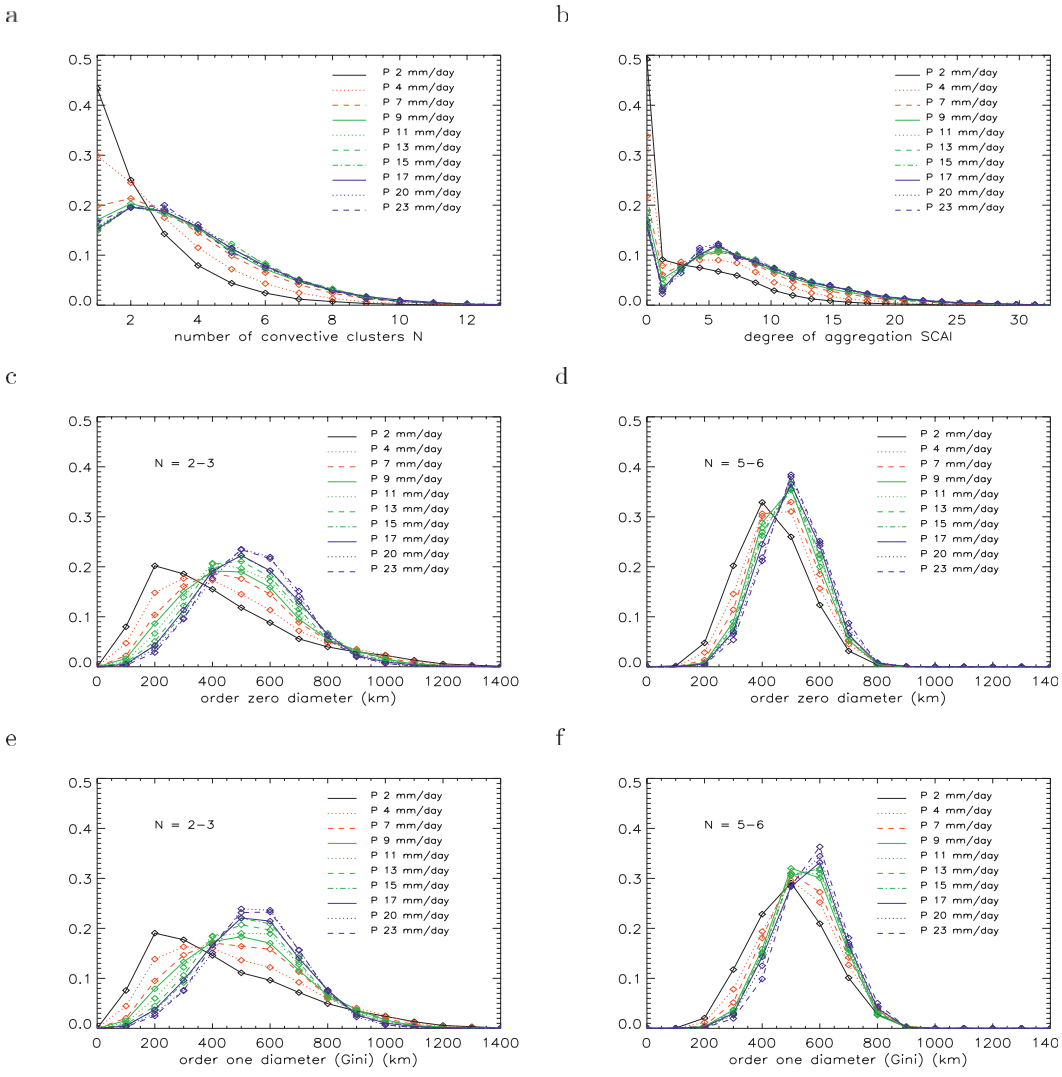

FIG. 3. (a) Normalized distributions of N within 10° × 10° domains sorted by precipitation regimes P above the Pacific Ocean for the period 1989–2005. The number of elements that make up the precipitation classes is from about 140 000 for $P = 2$ mm day^{-1} to 3200 for $P = 23$ mm day^{-1}. (b) As in (a), but for SCAI. (c)–(f) Normalized distributions of the distances D_0 and D_1 within 10° × 10° domains sorted by precipitation regimes P above the Pacific Ocean, for two given N classes, for the period 1998–2005.

instance, the squall line on 21 August 1992, observed during the Hydrological Atmospheric Pilot Experiment (HAPEX) campaign (Diongue et al. 2002) is associated with 1, 3, 2, 3, 1 clusters [respectively, D_0 of 0 (0 km), 0.24 (240 km), 0.32 (320 km), 0.53 (530 km), and 0 (0 km), and SCAI of 0, 3.6, 3.15, 7, and 0] every 3 h during its lifetime. Similarly, several tropical cyclones along their track, such as Hurricane Daniel on 25 July 2000 or Hurricane Hector on 14 August 2000 over the eastern Pacific, are characterized by a unique cluster along their track ($N = 1$; D_0 and SCAI values of 0).

The ability of the aggregation parameters to characterize the evolution of deep convective cloudiness in terms of the aggregation state is also examined. The first example is a diurnal evolution of high cloudiness over western Africa, which exhibits remarkable changes in aggregation (Fig. 5). In this case, N, D_0, and SCAI are computed over the entire domain under consideration (0°–20°N, 5°–30°E) rather than over 10° × 10° domains used elsewhere in this study. The N and SCAI diagnostics capture the main features of the variations in the aggregation state. Another example is the active phase of the January 1999 tropical intraseasonal oscillation occurring over the Indian Ocean (Fig. 6). The evolution of N (or SCAI) reveals an asymmetry of the active phase, which does not appear when simply

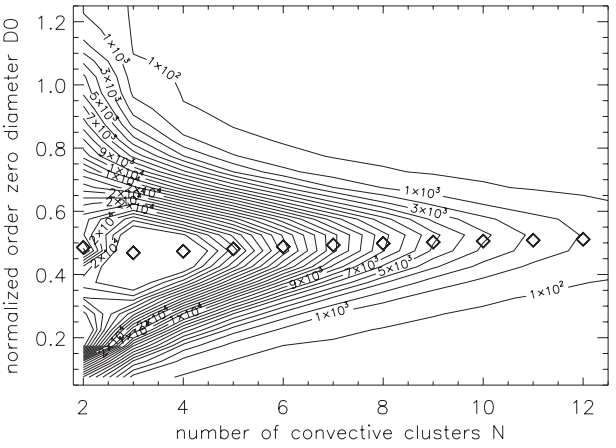

FIG. 4. Two-dimensional histogram of pairs (N, $\tilde{D}_0$) above the Pacific Ocean for the period 1988–2005 for all precipitation rates (for pairs with $N > 1$).

looking at the rain rate or at the deep convective cloudiness, commonly used to characterize the MJO. It indicates that the first step of the intensification phase consists of an increase in the number of the convective clusters (sections A–B, Fig. 6), then followed by an aggregation stage (B–C), during which systems become bigger and less numerous. Finally, the weakening stage (C–D) corresponds to states that are even more aggregated (at equivalent convective activity) than during the intensification stage (cf. days I and II in Fig. 6). This feature is consistent with the description of these phenomena by Duvel and Roca (2002). In both cases, changes in aggregation are primarily associated with changes in N.

Thus, this type of diagnostic makes it possible to characterize convective organization consistently with previous descriptions of observed convective organization.

4. Relationships between the degree of convective aggregation and the large-scale state of the atmosphere

This section presents the results of the compositing analyses of water vapor and energy fluxes by the aggregation parameters N, D_0, and SCAI.

a. Atmospheric humidity

1) DOMAIN AVERAGE

(i) Precipitable water

The relationship between precipitable water (PRW) and the number of clusters within the domain N is first examined (Fig. 7a) for each domain-averaged precipitation regime between 1 and 14 mm day^{-1} (beyond this regime, the statistical significance is too weak because of the constraints on large-scale conditions). The analysis reveals a sensitivity of PRW to N, which holds for all precipitation regimes: for low N (one or two clusters within the domain), the atmosphere is drier by about 1–2 kg m^{-2} (3%–5%) than when convection is split up into three to five clusters, and by about 2–4 kg m^{-2} (4%–8%) for higher N (more than five clusters). Thus, precipitable water and the number of convective clusters within the domain (or the density of clusters) are found to be correlated. Similarly, for given N classes, the D_0 compositing (Fig. 7b) reveals a sensitivity of PRW to the clumping of clusters, qualitatively consistent with the sensitivity to N. This sensitivity becomes significant for N higher than 3 (the clumping class of 0.15–0.4 is drier than the 0.65–0.9 class by 2–4 kg m^{-2}). Thus, a decrease in N can be compensated by an increase in D_0 with regard to PRW variations and vice versa. Figure 7b also shows that the sensitivity of PRW to N is slightly higher when D_0 is larger. This anticorrelation between PRW and convective aggregation is also found when using the combined parameter SCAI, which takes into account both features of aggregation (Fig. 7c). When comparing differences between the first and last quartiles of SCAI and N (or the first and last deciles) for different precipitation regimes, the sensitivity of PRW to SCAI is about 10% larger than the sensitivity to N.

(ii) Relative humidity profiles

To examine whether, for a given SST and large-scale dynamics, the observed modulation of PRW stems from specific levels of the atmospheric column, the relative humidity (RH) profiles from the ERA-Interim and AIRS datasets are composited by the aggregation parameters. In Fig. 8a, the ERA-Interim RH shows no sensitivity to N in the lower troposphere (up to about 850 hPa). Then, the profiles exhibit an absolute difference of 0.10–0.15 (15%–30% in relative difference) in the lower free troposphere over the range of N examined (from 1 to 11 clusters), which increases with altitude up to more than a 0.20 absolute difference (40%) above 400 hPa. AIRS satellite data show consistent results (Fig. 8b) despite a likely bias of AIRS data since no data are available in cloudy regions. However, AIRS data are characterized by a weaker sensitivity (by about 25% in the lower free troposphere to 50% in the mid- and upper troposphere compared to the ERA-Interim sensitivity; see Fig. 8c). The level of largest sensitivity also differs among datasets (e.g., above the Pacific Ocean, it occurs at 200 hPa for ERA-Interim versus 400 hPa for AIRS; see Fig. 8c) and among ocean basins (e.g., the ERA-Interim maximum level is around 300 hPa over the Indian Ocean). The analysis has also been conducted with National Centers for Environmental Prediction –National

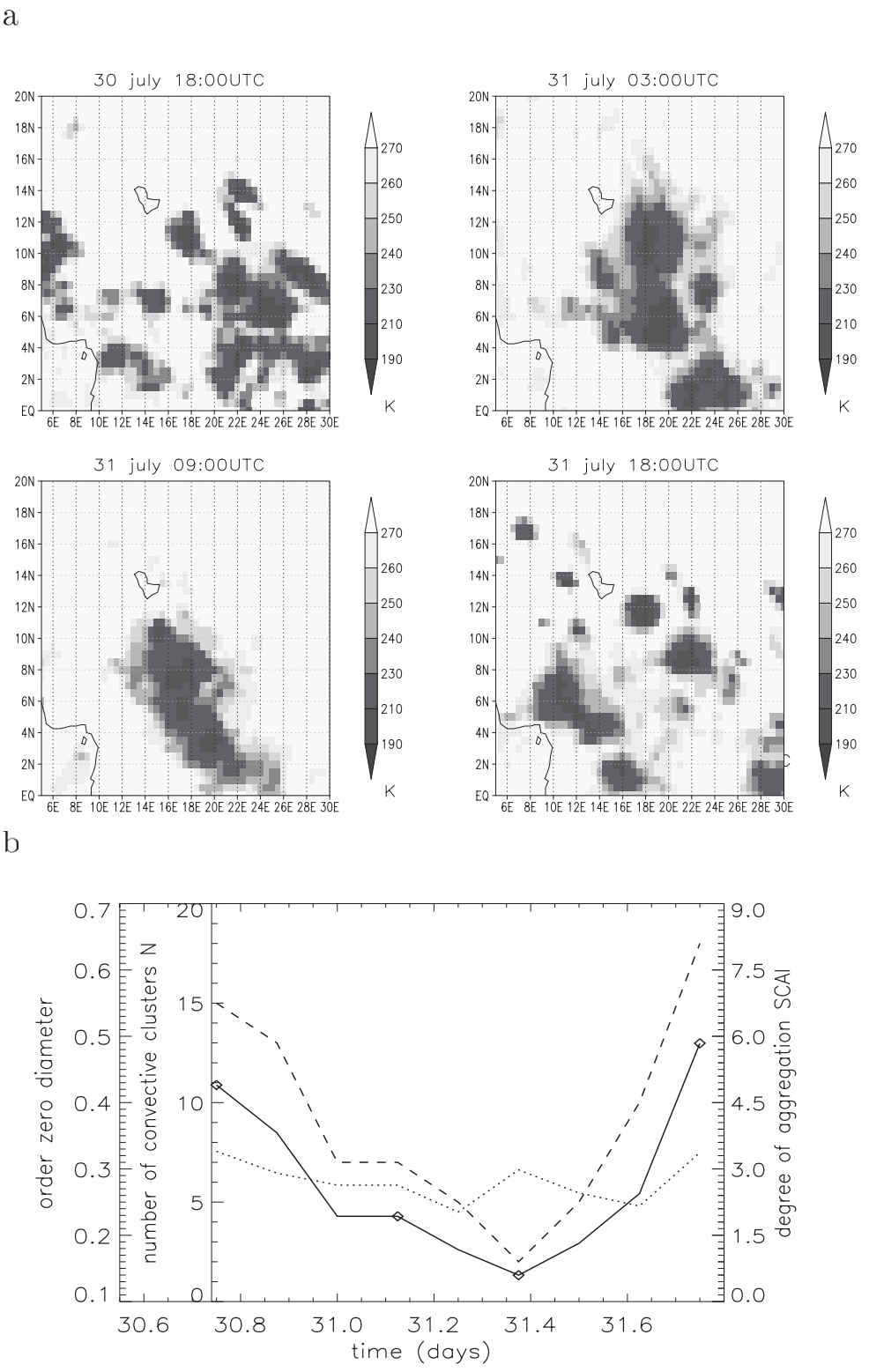

FIG. 5. (a) A sequence of CLAUS BT images over the African region 0°–20°N, 5°–30°E at (top left) 1800 UTC 30 Jul 2004, (top right) 0300 UTC 31 Jul 2004, (bottom left) 0900 UTC 31 Jul 2004, and (bottom right) 1800 UTC 31 Jul 2004. (b) Corresponding time series of N (dashed), $\tilde{D}_0$ (dotted), and SCAI (plain). The diamonds on the SCAI curve correspond to the CLAUS images shown. Note that the magnitude of the SCAI range depends on the size of the domain under consideration (mainly owing to the dependence of Nmax).

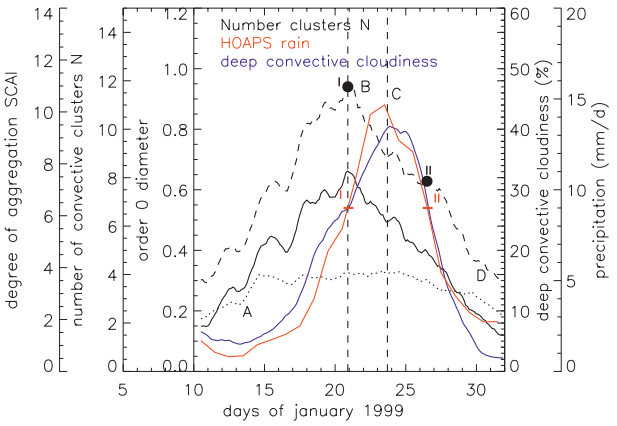

FIG. 6. Active phase of the January 1999 intraseasonal event over the Indian Ocean. The N, D_0, and SCAI parameters, the precipitation rate, and deep convective cloudiness are computed over the domain 0°–10°N, 75°–100°E. The curves are smoothed with a 4-day moving average.

Center for Atmospheric Research (NCEP–NCAR) reanalyses (Kalnay et al. 1996): these capture this anticorrelation between convective aggregation and humidity but to a lesser extent (not shown). Consistently, the D_0 compositing of RH from ERA-Interim reanalyses shows that for a given N, situations characterized by high clumping (D_0 of 0.15–0.4) are statistically drier in the midtroposphere (by about 0.05 or 10%) than those with lower clumping (D_0 of 0.65–0.9) (Figs. 8d,e). The analysis conducted with the combined parameter SCAI leads to the same findings as with N, qualitatively and quantitatively (Fig. 8f). As for PRW, RH results are not sensitive to which aggregation measure is used.

This analysis shows that the anticorrelation between aggregation and humidity primarily occurs in the free troposphere: for a given SST and large-scale vertical velocity, RH statistically increases with N, D_0, and SCAI above about 850 hPa with a maximum sensitivity above 500 hPa. These findings hold above all three tropical oceans, for all precipitation regimes (not shown).

2) DEEP CONVECTIVE CLOUDINESS AND HUMIDITY WITHIN AND OUTSIDE DEEP CONVECTIVE AREAS

To further analyze the relationship between the domain-averaged humidity and the degree of convective aggregation, the domain is now decomposed into two subdomains: the convective area (cv), made up of pixels with a brightness temperature colder than 240 K, whose extent is referred to as σ_{cv}, and the environment outside deep convection (ncv) (pixels warmer than 240 K). This analysis is conducted here with the N parameter but similar conclusions are obtained when using SCAI instead of N (not shown). For each N class, the mean characteristics over the domain $\overline{X}$ can be expressed to first order (the mean products of the fluctuations are of higher order):

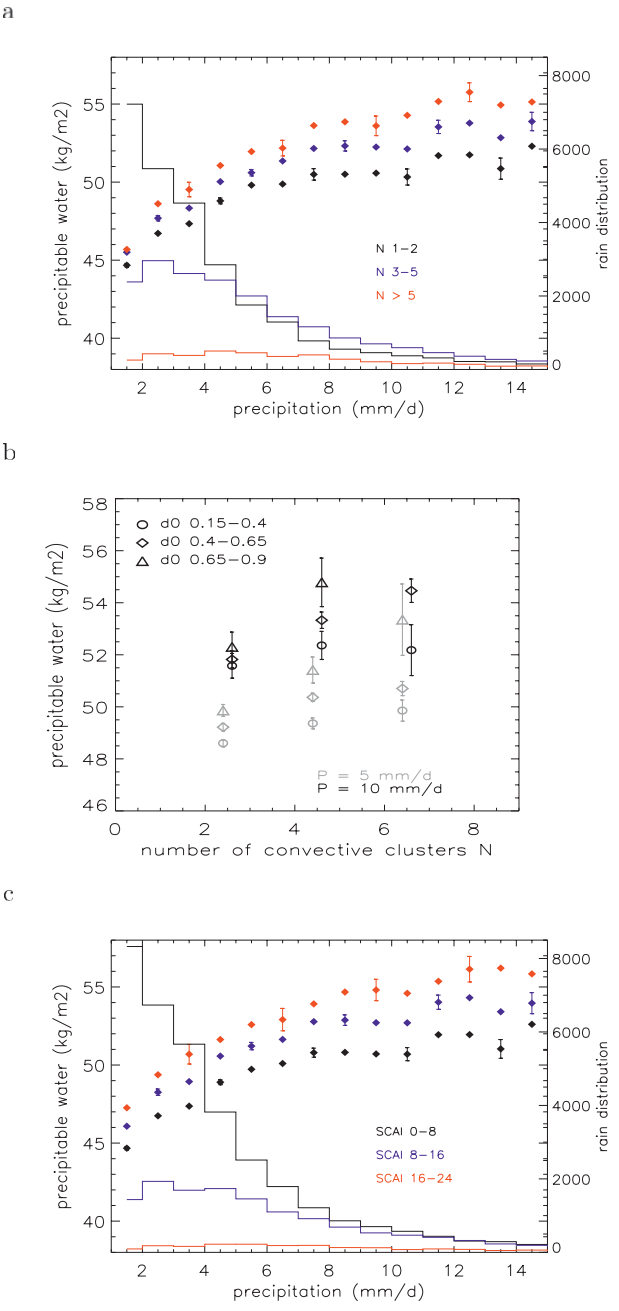

FIG. 7. (a) Precipitable water composited into precipitation bins of 1 mm day^{-1} for three N classes. (b) Precipitable water composited by D_0 and N for two precipitation rain rates. (c) As in (a), but for SCAI. The SST is constrained at 28°C. For each precipitation regime, the vertical velocity profiles are comparable among the aggregation classes. The few bars are the 95% confidence intervals. The precipitation histograms are shown in the backgrounds of (a) and (c).

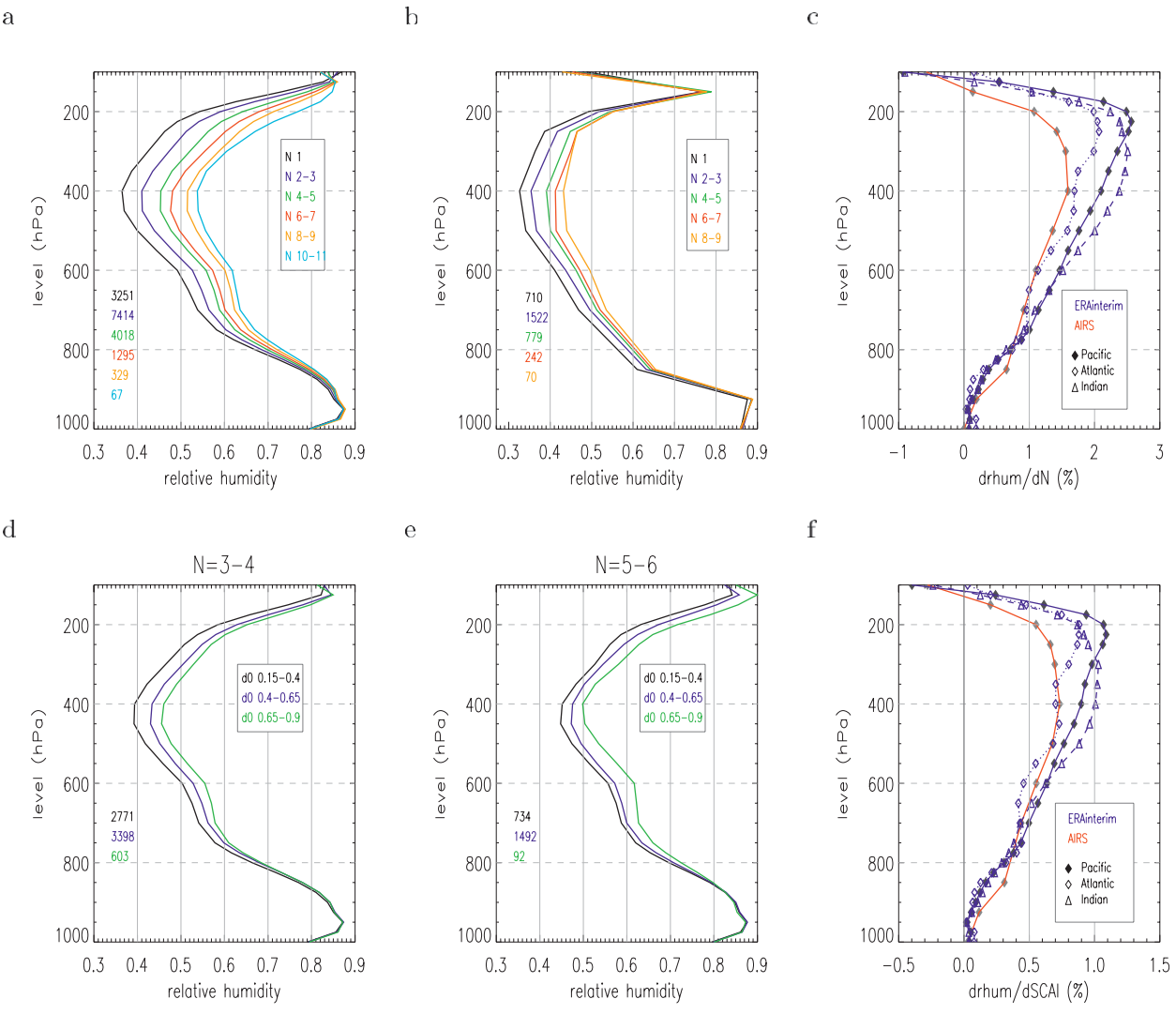

FIG. 8. RH profiles sorted by the aggregation parameters for a mean precipitation rate of 5 mm day^{-1}. (a) ERA-Interim RH stratified by N above the Pacific Ocean. (b) AIRS RH stratified by N above the Pacific Ocean. The sizes of the samples are indicated in the lower-left part of each graph. (c) Corresponding profiles of mean $\partial\overline{\mathrm{RH}}/\partial N$ for ERA-Interim (blue) for the three oceans and for AIRS (red). (d),(e) ERA-Interim RH stratified by D_0 for two N classes, above the Pacific Ocean. (f) Corresponding profiles of mean $\partial\overline{\mathrm{RH}}/\partial\mathrm{SCAI}$ for ERA-Interim (blue) for the three oceans and for AIRS (red). The composites are performed for given SSTs of 28°C (Pacific and Indian Oceans) or 27°C (Atlantic Ocean). The vertical velocity profiles are comparable among the aggregation classes.

$$[\overline{X}] = [\sigma_{\mathrm{cv}}][\overline{X_{\mathrm{cv}}}] + (1 - [\sigma_{\mathrm{cv}}])[\overline{X_{\mathrm{ncv}}}] \tag{2}$$

where brackets indicate the statistical mean within an N class and bars refer to the spatial averaging over the convective (cv) and nonconvective (ncv) regions, and the entire domain.

Variations in the domain-averaged humidity may result from differences in (i) the extent of the convective area, (ii) the humidity in the convective regions, and (iii) the humidity outside the convective regions:

$$\frac{\partial\overline{X}}{\partial N} = (\overline{X_{\mathrm{cv}}} - \overline{X_{\mathrm{ncv}}})\frac{\partial\sigma_{\mathrm{cv}}}{\partial N} + \sigma_{\mathrm{cv}} \times \frac{\partial\overline{X\mathrm{cv}}}{\partial N} + (1 - \sigma_{\mathrm{cv}})\frac{\partial\overline{X\mathrm{ncv}}}{\partial N}. \tag{3}$$

For a given precipitation rate, as N increases, deep convective cloudiness is more extended by a few percent (especially for weak precipitation regimes) (not shown). The precipitable water of the convective area varies little (which is expected since cloudy zones are dominated by

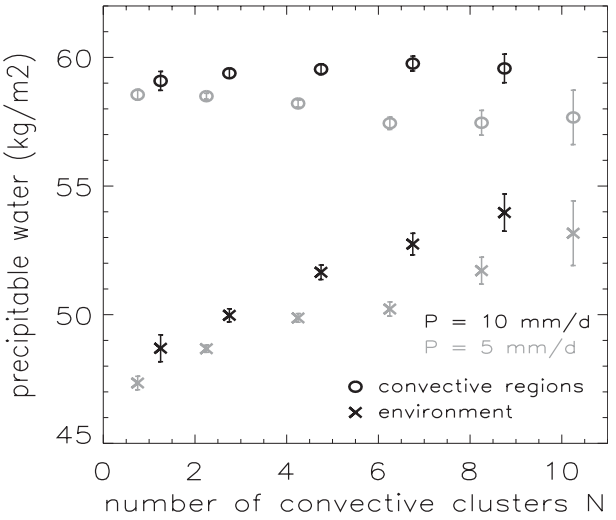

FIG. 9. Precipitable water averaged over the convective areas (circle) and over the nonconvective environment (cross) of the $10° \times 10°$ domains, composited by the N parameter, for two domain-averaged precipitation rates (5 and 10 mm day^{-1}). The composites are performed above the Pacific Ocean, for a given SST of 28°C. For each precipitation regime, the vertical velocity profiles are comparable among the N classes. The bars indicate the 95% confidence intervals.

saturated conditions and the temperature is fairly uniform in the tropical free troposphere) while that of the environment increases significantly (by about 15%) (Fig. 9). The quantification [using Eq. (3)] of the contribution of these different variations to $\partial\overline{X}/\partial N$ shows that the first two terms contribute very little while the last term accounts for about 95% of the total variation. Therefore, the anticorrelation between the domain-averaged humidity and aggregation primarily stems from the dryness of the environment outside convection when convection is more aggregated. Aggregated situations are thus characterized by stronger contrasts in humidity between deep convective and nonconvective regions.

b. Energetics

In addition to their strong interaction with humidity, which directly affects clear-sky radiative fluxes, convective processes play a key role in the sources and sinks of energy for the atmosphere, through a tight coupling with surface turbulent fluxes and cloud radiative effects. In this section, the relationships between convective organization and surface latent and sensible fluxes, as well as with radiative fluxes at the top of the atmosphere, are investigated.

1) SURFACE HEAT FLUXES

The N-compositing approach shows that total (latent and sensible) surface turbulent fluxes are very sensitive to the number of convective systems within the domain (Fig. 10a), with enhanced fluxes as the number of clusters decreases (15%–20% or about 20 W m^{-2} from 10 clusters to 1). This pattern of behavior characterizes sensible heat fluxes (40% difference) as well as latent heat fluxes (15% difference) (not shown). Consistently, the D_0-compositing approach (Fig. 10b) reveals that grouping of clusters leads to an enhancement of surface turbulent fluxes (by 10–15 W m^{-2} from 0.65–0.9 to 0.15–0.4 values of D_0) [this dependence is, however, less clear when the number of clusters is low (two or three clusters)]. Thus, the net effect on surface fluxes related to aggregation changes will depend on the relative change in N and D_0. For instance, in case of six to seven clusters with a clumping of 0.15–0.4, surface fluxes are stronger by about 20 W m^{-2} than those associated with four to five clusters with a clumping of 0.65–0.9. These relationships are confirmed by the SCAI-compositing method, which shows the strong covariance between surface turbulent fluxes and aggregation of convection (Fig. 10c). When comparing differences between the first and last quartiles of SCAI and N (and the first and last deciles) for different precipitation regimes, the sensitivity of surface fluxes to SCAI is about 25%–30% higher than the sensitivity to N.

These findings are further analyzed by examining deep convective and nonconvective areas separately [Eqs. (2) and (3)], as is done for humidity. Here, N is used, but our conclusions are very similar when using SCAI. In both areas surface sensible and latent fluxes exhibit a sensitivity to the number of clusters (or convective aggregation), stronger in deep convective areas than in the environment (varying from 40 to 20 W m^{-2} over the range of N examined) (Fig. 10d). The contribution of deep convective regions to the domain-averaged sensitivity is proportional to the deep convective cloudiness and thus depends on the precipitation regime (e.g., deep convection regions contribute to 30% of the total variation for 20 mm day^{-1} rain rates, while for weak precipitation regimes, the contribution is only of a few percent). The contribution of the environment remains dominant because of its larger area. Note that the fluxes are stronger in convective areas than in the environment by more than 20 W m^{-2} regardless of the number of clusters, suggesting an enhancement of surface fluxes by convective systems, as highlighted by Jabouille et al. (1996) and Saxen and Rutledge (1998). As a result, unlike humidity, the decrease in the deep convective area as the number of clusters decreases tends to weaken the sensitivity of the domain-averaged turbulent fluxes to N (or to the aggregation state) by a few percent.

As expressed by the bulk formula of the turbulent fluxes [Eq. (4)], the latent heat flux Q_L is proportional to the surface wind speed V and the difference between the

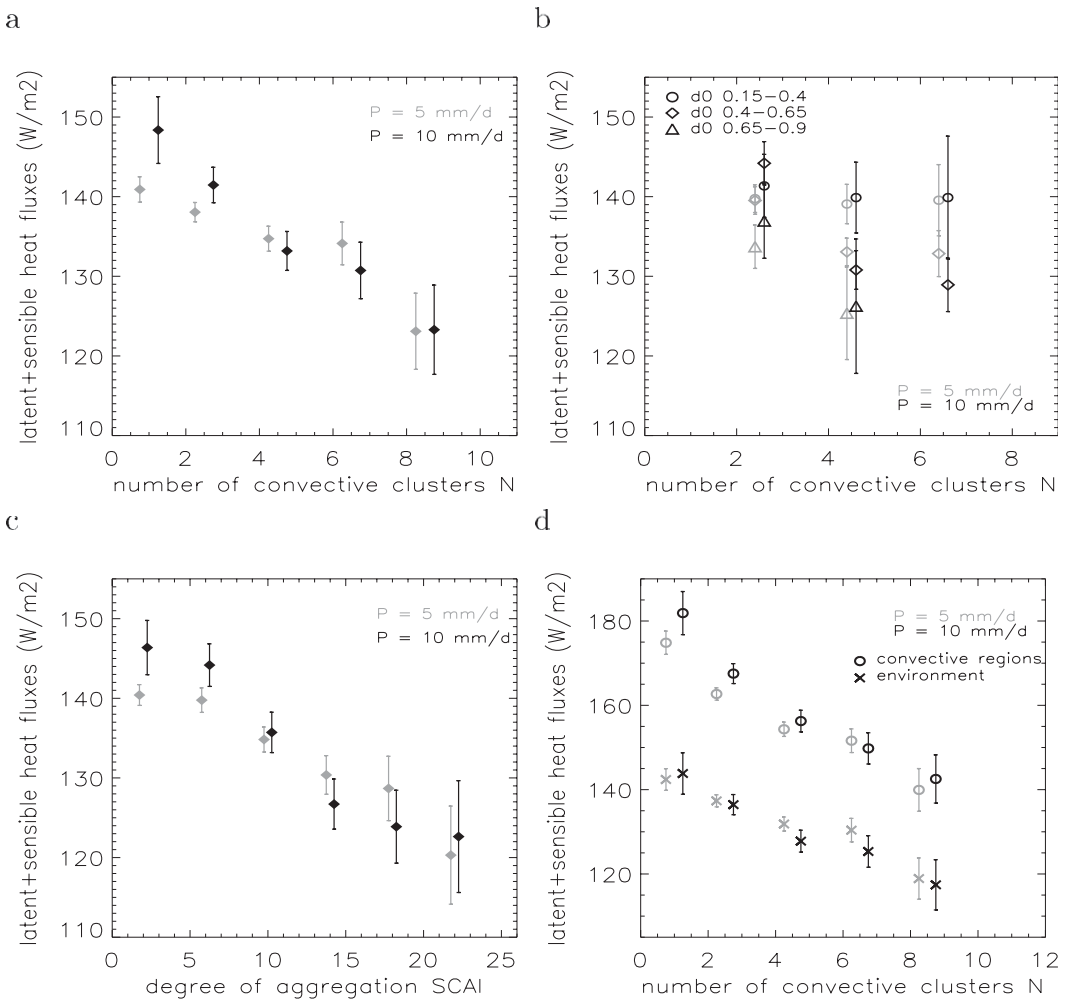

FIG. 10. (a) The 10° × 10° domain-averaged total surface turbulent heat fluxes (latent + sensible) composited by N for two domain-averaged precipitation rates. (b) Total surface fluxes stratified by D_0 and N for two domain-averaged precipitation rates. (c) As in (a), but for SCAI. (d) As in (a), but for surface fluxes of convective (circle) and nonconvective regions (cross) separately. The composites are performed above the Pacific Ocean, for a given SST of 28°C. For each precipitation regime, the vertical velocity profiles are comparable among the aggregation classes. The bars indicate the 95% confidence intervals.

sea surface saturation specific humidity and the near-surface specific humidity, Δhum. To understand the relationships between surface turbulent fluxes and the number of clusters both in convective and nonconvective regions, the 10-m wind speed (V) and Δhum are composited into N classes for precipitation regimes of 5 and 10 mm day^{-1} (not shown). At first order, the variations in mean fluxes as a function of N result from a difference in mean V and mean Δhum with N [Eq. (5)]

$$Q_L = \rho_a C_d L V \Delta\text{hum} = KV\Delta\text{hum}, \tag{4}$$

where ρ_a, C_d, and L are, respectively, the air density (ρ_a = 1.2 kg m^{-3}), the drag coefficient (C_d = 1.4 × 10^{-3}), and the specific latent heat of vaporization (L = 2.5 × 10^6 J kg^{-1}):

$$\frac{\partial\overline{Q_L}}{\partial N} = K\overline{V}\frac{\partial\overline{\Delta\text{hum}}}{\partial N} + K\overline{\Delta\text{hum}}\frac{\partial\overline{V}}{\partial N}. \tag{5}$$

In convective areas, the wind speed and Δhum increase regularly with convective aggregation [by 15% (more than 1 m s^{-2}) and 7%–8% (0.4 g kg^{-1}), respectively, from nine clusters to a unique cluster]. In the nonconvective region, the wind speed increases less than in convective regions (by about 5%–7%) and Δhum increases with convective aggregation by about 10% from nine clusters to one. Thus, in convective (nonconvective) regions, the variations in V contribute to 65%–70%

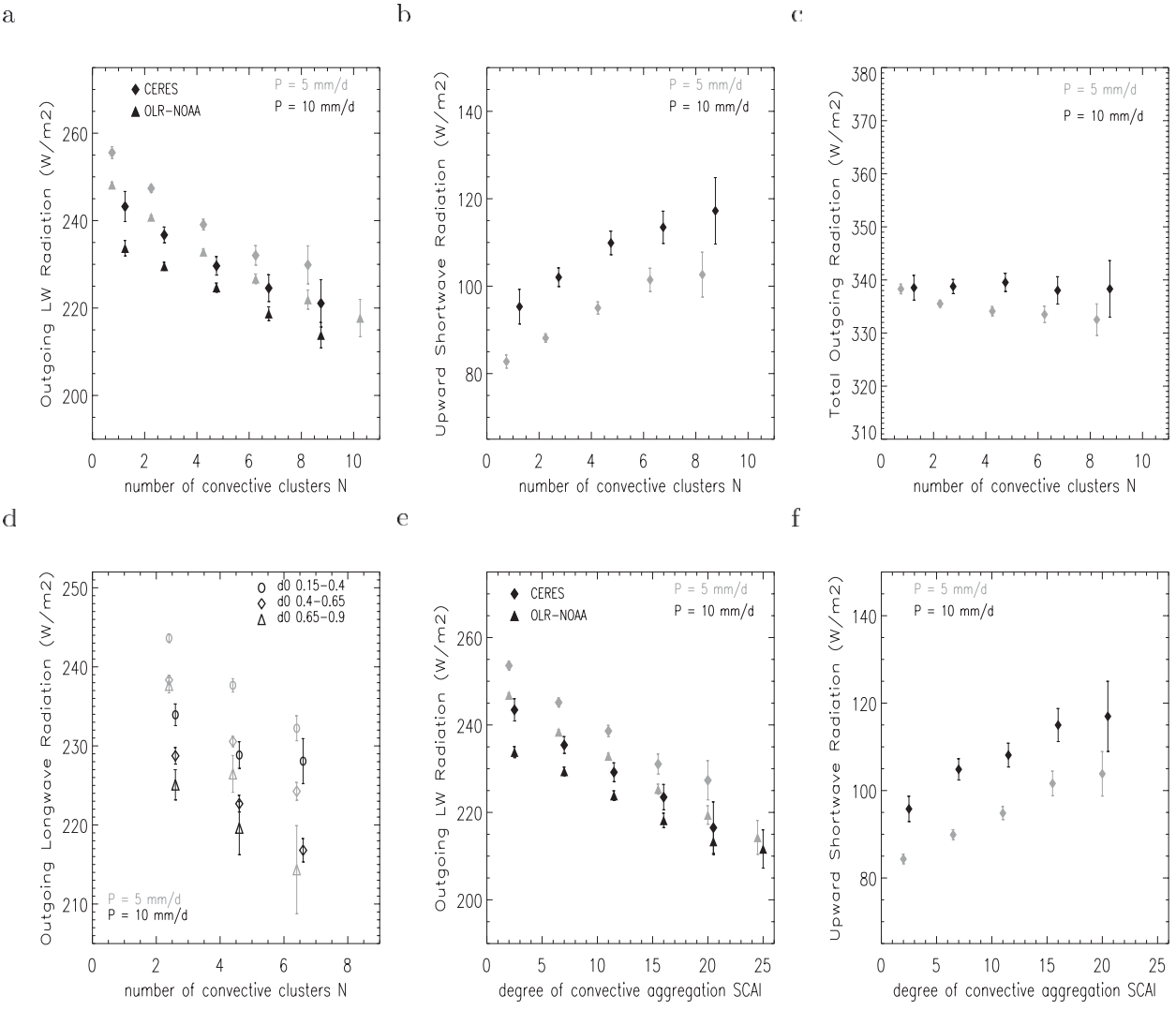

FIG. 11. (a) The N composites of OLR flux at the TOA for the CERES (diamonds) and OLR-NOAA (triangle) datasets, for two domain-averaged precipitation rates. (b) As in (a), but for outgoing shortwave radiation at the TOA. (c) As in (a), but for the total outgoing radiative fluxes. (d) OLR stratified by D_0 and N. (e) As in (a), but for SCAI. (f) As in (b), but for SCAI. The composites are performed above the Pacific Ocean, for a given SST of 28°C. For each precipitation regime, the vertical velocity profiles are comparable among the aggregation classes. The bars indicate the 95% confidence intervals.

(25%–40%) of the total flux variations and the variations in Δhum account for 30%–35% (60%–75%). Therefore, convective aggregation is accompanied by stronger turbulent energy exchanges between the ocean and the atmosphere because of enhanced near-surface wind speed and air–sea differences; the wind speed effect prevails in convective regions while the air–sea difference effect prevails in nonconvective regions.

2) TOA RADIATIVE FLUXES

The differences in atmospheric humidity that accompany the differences in the convective aggregation state are likely to affect the radiative fluxes at the top of the atmosphere and, thus, the energy budget of the atmosphere. This is examined by first compositing the outgoing longwave radiation (OLR) by aggregation parameters. The OLR appears to covary strongly with the number of clusters: from the least to most aggregated N class, OLR is enhanced by up to 30 W m^{-2} (Fig. 11a). An increase in the clumping of clusters (from D_0 of 0.65–0.9 to 0.15–0.4) also leads to an increase in OLR of 10–20 W m^{-2} (Fig. 11d). These relationships are summarized by the SCAI compositing of OLR (Fig. 11e), which corroborates the correlation between OLR and convective aggregation. Although both datasets (OLR-NOAA and CERES) differ systematically from each other by

TABLE 2. Percentage of cloud coverage at different altitudes (defined as the fraction of CLAUS pixels having a brightness temperature BT within a certain range of temperatures) over a 10° × 10° domain composited by (top) N and (bottom) SCAI, for an instantaneous domain-averaged precipitation rate of 5 mm day^{-1}. The composites are performed above the Pacific Ocean, for a given SST of 28°C. The vertical velocity profiles are comparable among the aggregation classes.

N	1	2–3	4–5	6–7	8–9
BT ≥ 285 K	64%	56%	47%	39%	33%
260 ≤ BT < 285 K	22%	24%	27%	29%	30%
240 ≤ BT < 260 K	8%	12%	17%	22%	26%
BT < 240 K	6%	8%	9%	10%	11%
SCAI	0–6	6–12	12–18	18–24	24–30
BT ≥ 285 K	62%	54%	48%	39%	31%
260 ≤ BT < 285 K	22%	24%	27%	29%	32%
240 ≤ BT < 260 K	10%	14%	17%	22%	25%
BT < 240 K	6%	8%	8%	10%	12%

about 7 W m^{-2}, both reveal a similar sensitivity to aggregation.

Such a sensitivity, however, cannot result from a clear-sky humidity difference. Indeed, for relative humidities of 30%–60% (Fig. 8), a 20% difference in free-tropospheric humidity would lead to no more than 10 W m^{-2} differences (Spencer and Braswell 1997; Roca et al. 2011). Therefore, since clouds strongly interact with longwave radiation, the dependence of the cloud cover on the degree of convective aggregation needs to be examined. As for deep convective cloudiness, brightness temperature is used to estimate the cloud amount at lower altitudes. Table 2 indicates that deep convective cloudiness is less extended for aggregated convection than for scattered convection, as has already been mentioned in section 4a(2). This is consistent with the fact that anvils of connected MCSs are less extended than those of separated MCSs (Yuan and Houze 2010). The shallow and midlevel cloud amounts also decrease with convective aggregation, which is consistent with the decrease in humidity. Convective aggregation is thus accompanied by more extended clear-sky regions over the domain (approximately doubled over the ranges of N or SCAI explored). Therefore, OLR variations with convective aggregation primarily result from changes in both deep convective and nonconvective cloud cover.

Changes in cloud amount also imply an effect on the reflected shortwave radiation (RSW). Figures 11b and 11f show that RSW is correlated with N (or SCAI). This dependence of RSW on aggregation parameters, which corresponds to a 5% change in planetary albedo of the domain over the range of N (or SCAI) considered, is quantitatively comparable to that of OLR (the sensitivity of RSW to the clumping of clusters cannot be examined because of poor statistics).

Due to these opposing effects, the TOA energy budget is not significantly different among the convective aggregation states (Fig. 11c). Nevertheless, the radiative heating distribution through the atmosphere is presumably considerably modulated because shortwave radiation primarily heats the surface while longwave radiative heating occurs mostly through the troposphere. Consequently, the large-scale circulation is likely to be affected by the aggregation state of convection.

5. Conclusions

a. Summary of main findings

Tropical deep convection exhibits complex organization from the mesoscale to the planetary scale. Convective organization is addressed here in terms of the aggregation state at the synoptic scale. The implications of the convective aggregation for the large-scale atmospheric state have been the focus of several cloud-resolving model (CRM) studies (e.g., Held et al. 1993; Tompkins 2001; Bretherton et al. 2005; Khairoutdinov and Emanuel 2010). This study uses observations to address this issue. A simple and objective method for characterizing the degree of convective aggregation is introduced. This method consists of using satellite infrared brightness temperature images to compute the mean density and the clumping of convective clusters within 10° × 10° domains. The analysis has been conducted above tropical oceans, using long time series of several satellite and reanalysis datasets. Statistical relationships between the degree of convective aggregation and water vapor and energy fluxes have been highlighted:

(i) A robust anticorrelation is found between convective aggregation and free-tropospheric humidity, stemming from the environment outside deep convective regions, especially in the middle and upper troposphere (up to a 0.2 absolute effect on RH).
(ii) Surface turbulent (latent and heat) fluxes are also found to be enhanced in situations of more aggregated convection (i.e., by 20% or 20 W m^{-2}), both within and outside deep convective regions. This enhancement in surface fluxes is mainly due to increased surface wind in convective regions and to an increase in air–sea humidity differences in the environment.
(iii) Radiative fluxes at the TOA are highly sensitive to the aggregation state of convection. More longwave radiation (OLR) escapes from the system when convection is more aggregated (up to 30 W m^{-2} increase). Humidity differences (which are maxima

at the levels where OLR is the most sensitive to RH changes) contribute to OLR differences but do not constitute the primary cause of OLR variations because RH changes do not strongly affect the OLR when the free troposphere is fairly moist (relative humidities of 30%–60%) (Spencer and Braswell 1997; Roca et al. 2011). The present analysis shows that, as convective aggregation increases, the significant reduction (by half in total) in cloudiness at all levels is primarily responsible for this strong OLR increase. The reflected shortwave radiation is also substantially reduced and, thus, the TOA net radiative budget is not significantly affected by the degree of convective aggregation. Nevertheless, the vertical distribution of the radiative heating through the atmosphere is affected, which is a forcing for the large-scale circulation. Consequently, the latter is likely to be modulated by the degree of convective aggregation.

This analysis has revealed significant relationships between atmospheric variables and both the number and the clumping of convective clusters. To first order, however, the atmospheric variables are more strongly associated with the number of clusters. This is because, within the present observational framework, the variability of the clumping of clusters is weak (cf. Figs. 3 and 4). This partly results from geometrical reasons (finite size of the clusters and limited size of the domains), but it may also have physical causes such as the ability of convective systems to inhibit or favor neighboring systems. Within a different framework (modeling) or in a different climate, the variability of the clumping of clusters may differ. Given the potential role of this parameter in the atmospheric state variability, it may be important to consider as a supplement to the number of clusters when carrying out this type of study.

b. Discussion

1) METHODOLOGY

The potential limitations of this observational study, associated with both the methodology and the data used, have been examined. Main points are presented here.

- IR instruments cannot measure through clouds. To ensure the reliability of the HOAPS SST data, derived from IR measurements, this dataset has been compared to the optimally interpolated (OI) SST dataset, derived from microwave measurements and thus making it possible to measure the SSTs under clouds. Some biases are identified for SSTs higher than 29°C, but the correction of these biases does not affect the results (not shown).
- During strong precipitation events, the retrieval of near-surface wind speed, turbulent fluxes, or precipitable water is not possible or requires some corrections. This might affect observational results primarily related to convective cores. The signals reported here, however, are dominated by changes outside convective cores. They are thus unlikely to be affected by this limitation.
- The coincidence of the different datasets is not perfectly achieved, especially when relating the instantaneous convective state from CLAUS data to daily radiative longwave and shortwave fluxes data. The same conclusions, however, are obtained when a daily averaged aggregation index is related to daily radiation data. Indeed, the daily variance of the aggregation parameters is quite small over tropical oceans (especially compared to land regions), which might be due to the longer lifetime of convective systems over oceans than over lands (Houze 2004).
- A number of arbitrary selections of parameters have been made, such as the tolerated amount of missing data within $10° \times 10°$ domains, the connectivity between pixels, the convective brightness temperature (BT) threshold, and the formula for the aggregation index. As mentioned in the paper, however, our findings are not sensitive to these choices.
- Using the deep convective area (σ_{cv}), defined by pixels colder than 240 K, as the proxy for convective activity instead of the precipitation rate also leads to the same findings. This is consistent with the fact that, for a given precipitation rate, σ_{cv} changes very little among the degrees of aggregation. The main difference is a reduced sensitivity of TOA radiation to convective aggregation when σ_{cv} is used. The choice of the precipitation rate is, however, preferred because this variable is much more constrained by climate equilibria than is the cloud amount. Moreover, it allows us to reveal the tendency of aggregated convection to be slightly less horizontally extended than scattered convection.
- The clustering over a limited domain frequently leads to the disregard of whole clusters at the edges of the domains. Repeating the analysis by considering only the domains that include full clusters leads to drastically reduced statistics, but does not affect the results.
- Finally, the 0.5° spatial resolution of the CLAUS dataset used is quite coarse and does not make it possible to capture isolated thunderstorm cells (a few kilometers). A cold pixel is already considered to correspond to an MCS. The analysis has been repeated with the much higher-resolution BT dataset of Meteosat (5-km resolution; every 30 min) over the Atlantic Ocean. The findings of the study are well confirmed qualitatively and quantitatively (see Table 3). The Meteosat dataset is not used for this study because it is less convenient to handle than low-resolution datasets for a long time

TABLE 3. Differences (δQ) between the 15% least aggregated (Q_{sup}) and the 15% most aggregated (Q_{inf}) classes ($\delta Q = Q_{sup} - Q_{inf}$), derived from Meteosat and CLAUS data for precipitable water (PRW, kg m^{-2}), RH at 500 and 300 hPa (rhum500, rhum300; %), turbulent fluxes (LATE + HEAT, W m^{-2}), and OLR (W m^{-2}). The precipitation regime is about 10 mm day^{-1}. The analyzed region is the tropical Atlantic Ocean.

	δQ PRW	δQ rhum500	δQ rhum300	δQ LATE + HEAT	δQ OLR
CLAUS	3	10.5	12	−8.5	−19
Meteosat	3.1	9.8	17.5	−8	−17

period and a large fraction of the globe (all tropical oceans).

- The analyses have been repeated using the vertical velocities from NCEP–NCAR reanalyses (Kalnay et al. 1996). The results are qualitatively similar to the ones obtained by using ERA-Interim vertical velocity but the sensitivity of the climatological variables to the degree of convective aggregation is increased by 25%–35%.

The insensitivity of the results to these choices and to most of the limitations, as well as the strong consistency among all datasets (which are derived from independent instruments), both give confidence in the robustness of our findings. However, it would be worth repeating the analysis with other datasets such as the Tropical Rainfall Measuring Mission (TRMM; Liu et al. 2007) for better characterizing convective precipitation, active datasets such as Cloud–Aerosol Lidar and Infrared Pathfinder Satellite Observations (CALIPSO; Winker et al. 2009) for better characterizing changes in cloud types, or even the future products of the recently launched *Megha-Tropiques* satellite (Roca et al. 2010) for improving both the spatiotemporal sampling and coincidence of precipitation, radiative fluxes, and water vapor measurements over the tropics.

2) PHYSICAL MECHANISMS

The findings of this study are qualitatively consistent with previous CRM studies, with regard to humidity (Held et al. 1993; Tompkins 2001; Bretherton et al. 2005; Khairoutdinov and Emanuel 2010), surface fluxes (Bretherton et al. 2005), and OLR (Held et al. 1993; Bretherton et al. 2005, Khairoutdinov and Emanuel 2010). Moreover, the analysis of mean precipitation in convective areas has shown that aggregated convection is statistically characterized by more intense rainfall events at the mesoscale than scattered convection (not shown), which is also in agreement with Bretherton et al. (2005). The results related to surface turbulent fluxes are also consistent with previous observational studies (Saxen and Rutledge 1998; Jabouille et al. 1996; Young et al. 1995).

Although determining cause and effect relationships between convective aggregation and humidity is not obvious when using observations, a positive feedback is likely to operate. Under the convection–humidity positive feedback (e.g., Tompkins 2001; Grabowski 2003), a dry atmosphere is not favorable for deep convection to develop in many spots. In turn, the localization of convection limits horizontal mixing between deep convective regions and the large-scale environment outside convection (Held et al. 1993; Tompkins 2001). This results in maintaining the dryness of the regions surrounding deep convection and allows the convection–moisture feedback to operate efficiently, which may amplify the dry conditions in subsiding areas. Efficient mesoscale circulations that transport moist static energy from dry to moist regions may also enhance the contrasts between both regions (Bretherton et al. 2005). Those CRM studies suggest that the absence of tropospheric vertical wind shear is essential for the interaction between convective organization and tropospheric humidity to operate efficiently. In our case, over oceans, the analysis of NCEP wind profiles shows that weak or no wind shear conditions are prominent over tropical oceans, which justify the comparison and the consistency with CRMs findings.

In addition, the clustering of convection may increase the precipitation efficiency by protecting convective mass fluxes from the environment and thus limiting the entrainment of unsaturated air along with rain evaporation. Clumped convection is hereby likely to be associated with more intense rainfall events than scattered convection. Indeed, the precipitation efficiency of convective clusters, as calculated by the ratio of the precipitation rate over the boundary layer precipitable water, $P/\mathrm{PRW}_{\mathrm{BL}}$ (Del Genio and Kovari 2002), increases with convective aggregation, since in convective regions precipitation rates are higher while boundary layer precipitable water does not differ from scattered convection. Less condensate is then detrained in the free troposphere, which may result in less extended anvils of convective systems and in a decrease in the mean atmospheric moisture.

The enhancement of turbulent surface fluxes in convective regions as convective aggregation increases can be related to the observed dependence of surface fluxes

on the mode of convective organization (Saxen and Rutledge 1998); that is, highly organized systems produce larger enhancement of surface fluxes than does less organized convection. This effect could imply a modulation of mean surface fluxes at larger scales [Jabouille et al. (1996) show it at a smaller scale than in the present study]. Cold pools formed under convective systems, whose characteristics are likely to be affected by convective organization, may play a role in the modulation of surface fluxes intensity, through the generation of gust winds and air–sea differences (Young et al. 1995). Depending on their extent, cold pools can also more or less influence the environment. Environmental enhancement of fluxes in aggregated situations may also be induced by mesoscale circulations (Bretherton et al. 2005), as well as by the increase in air–sea difference.

Observational results and CRM studies disagree on the causes of OLR increase when convection is more aggregated. The reduction in environmental cloudiness that prevails in observations is not reproduced in CRMs studies, which solely invoke the clear-sky humidity effect on radiation. The observed compensating effect of convective aggregation on reflected shortwave radiation (SW) and OLR is not found in CRM simulations: either the SW effect is not considered (Khairoutdinov and Emanuel 2010) or it is found to amplify the OLR effect, owing to an increase in low-level clouds in the regions surrounding deep convection (Held et al. 1993).

c. *Implications and outlook*

The diagnostic of convective aggregation presented in this paper would be easily applicable to the OLR field or simulated BT of CRM simulations (Diongue et al. 2002). It would be possible to compare quantitatively modeling and observational results in order to point out the performance and the shortcomings of CRMs with regard to convective organization, such as the effect on mid- and low-level cloudiness and reflected shortwave radiation.

The strong interaction between the degree of convective aggregation and the large-scale state, revealed by this observational study, has implications for climate modeling. The present work suggests that a good representation of 1) convective organization and 2) the relationships between convective organization state and mean state may be required for simulating a realistic large-scale state in terms of water vapor and energy fluxes. It might also be important for the simulation of the climate variability such as the Madden–Julian oscillation (MJO) (cf. Fig. 6), for which convection–humidity feedback plays an important role (Grabowski and Moncrieff 2004; Bony and Emanuel 2005). The representation of tropical convective organization, however, remains a challenge for general circulation models (GCMs) at most scales: at the 50–300-km scale (grid-box sizes), the mesoscale organization of convection is not represented in current convection parameterizations and the large-scale (explicitly resolved) organization of convection, such as the MJO, is still poorly simulated in many GCMs (Lin et al. 2006). In addition, the difficulties of models relative to moisture–convection interactions (Derbyshire et al. 2004), cloud representation, and other processes are likely to impact the relationships between convective organization and the mean state. These deficiencies may be a source of systematic biases in the simulated mean state, such as the biased precipitation–humidity relationship (Biasutti et al. 2006) or in the simulation of climate variability such as the MJO.

The diagnostic of convective aggregation may be applied to high-resolution GCMs in order to evaluate the representation of convective organization and its interaction with water vapor and energy fluxes. Whether convective organization at synoptic resolved scales requires a realistic representation of convective organization at subgrid scales remains an open issue. Some attempts to include features of mesoscale convective organization in parameterization schemes have been carried out (Moncrieff 2004; Qian et al. 1998; Redelsperger et al. 2000; Grandpeix and Lafore 2010; Mapes and Neale 2011). By using the diagnostic of convective aggregation, it would be informative to analyze the impact of these efforts on the representation of convective organization and its relationships with the mean climate state in these GCMs.

The aggregation state of convection presumably affects the interaction of convection with atmospheric humidity and cloudiness, by modulating features such as precipitation efficiency, precipitation evaporation, or entrainment and detrainment characteristics. Changes in the aggregation state of convection have hence the potential to affect the atmospheric circulation and its organization over a large range of scales (Slingo and Slingo 1988; Randall et al. 1989; Zurovac-Jevtic et al. 2006; Kang et al. 2008). Therefore, a ''convective organization feedback'' might play a role in climate variability and change. This possibility will be examined in a future study.

Acknowledgments. We are grateful to J.-Y. Grandpeix for his help in the intellectual seeds of this work and fruitful comments throughout the course of this study. We also wish to thank J.-P. Lafore and S.C. Sherwood for stimulating discussions. We acknowledge N. Gauvrit for useful exchanges on the ''order zero diameter'' and for his interest in our work. We also thank A. Andersson for their helpful exchanges on HOAPS data. Karim Ramage and Sophie Cloche are acknowledged for their assistance and for providing datasets used for this study via

ClimServ. The thoughtful comments of two anonymous reviewers helped us to reorganize and improve the paper. This work is partly supported by the LEFE MISTERRE national program.

REFERENCES

Andersson, A., K. Fennig, C. Klepp, S. Bakan, H. Graßl, and J. Schulz, 2010: The Hamburg Ocean Atmosphere Parameters and Fluxes from Satellite Data HOAPS-3. *Earth Syst. Sci. Data,* **2,** 215–234, doi:10.5194/essd-2-215-2010.

Aumann, H., and Coauthors, 2003: AIRS/AMSU/HSB on the Aqua mission: Design, science objectives, data products, and processing systems. *IEEE Trans. Geosci. Remote Sens.,* **41,** 253–264.

Biasutti, M., A. Sobel, and Y. Kushnir, 2006: AGCM precipitation biases in the tropical Atlantic. *J. Climate,* **19,** 935–958.

Bony, S., and K. Emanuel, 2005: On the role of moist processes in tropical intraseasonal variability: Cloud–radiation and moisture–convection feedbacks. *J. Atmos. Sci.,* **62,** 2770–2789.

——, K. Lau, and Y. Sud, 1997: Sea surface temperature and large-scale circulation influences on tropical greenhouse effect and cloud radiative forcing. *J. Climate,* **10,** 2055–2077.

Bretherton, C., P. Blossey, and M. Khairoutdinov, 2005: An energy-balance analysis of deep convective self-aggregation above uniform SST. *J. Atmos. Sci.,* **62,** 4273–4292.

Del Genio, A., and W. Kovari, 2002: Climatic properties of tropical precipitating convection under varying environmental conditions. *J. Climate,* **15,** 2597–2615.

Derbyshire, S., I. Beau, P. Bechtold, J.-Y. Grandpeix, J. Piriou, J.-L. Redelsperger, and P. Soares, 2004: Sensitivity of moist convection to environmental humidity. *Quart. J. Roy. Meteor. Soc.,* **130,** 3055–3079.

Diongue, A., J. Lafore, J. Redelsperger, and R. Roca, 2002: Numerical study of a Sahelian synoptic weather system: Initiation and mature stages of convection and its interactions with the large-scale dynamics. *Quart. J. Roy. Meteor. Soc.,* **128,** 1899–1927.

Duvel, J.-P., and R. Roca, 2002: Intra-seasonal perturbation of the convective activity over the Indian Ocean and relationships with SST. Preprints, *25th Conf. on Hurricanes and Tropical Meteorology,* San Diego, CA, Amer. Meteor. Soc., 16B.2. [Available online at http://ams.confex.com/ams/pdfpapers/32566.pdf.]

Gauvrit, N., and J.-P. Delahaye, 2006: Order 0 diameter. A ''natural'' measure of scattering. *Math. Sci. Hum.,* **175,** 41–51.

Grabowski, W., 2003: MJO-like coherent structures: Sensitivity simulations using the cloud-resolving convection parameterization (CRCP). *J. Atmos. Sci.,* **60,** 847–864.

——, and M. Moncrieff, 2004: Moisture–convection feedback in the tropics. *Quart. J. Roy. Meteor. Soc.,* **130,** 3081–3104.

Grandpeix, J., and J. Lafore, 2010: A density current parameterization coupled with Emanuel's convection scheme. Part I: The models. *J. Atmos. Sci.,* **67,** 881–897.

Held, I., R. Hemler, and V. Ramaswamy, 1993: Radiative–convective equilibrium with explicit two-dimensional moist convection. *J. Atmos. Sci.,* **50,** 3909–3909.

Hodges, K. I., D. W. Chappell, G. J. Robison, and G.-Y. Yang, 2000: An improved algorithm for generating global window brightness temperatures from multiple satellite infrared imagery. *J. Atmos. Oceanic Technol.,* **17,** 1296–1313.

Houze, R., Jr., 1977: Structure and dynamics of a tropical squall-line system. *Mon. Wea. Rev.,* **105,** 1540–1567.

——, 2004: Mesoscale convective systems. *Rev. Geophys.,* **42,** RG4003, doi:10.1029/2004RG000150.

Jabouille, P., J. Redelsperger, and J. Lafore, 1996: Modification of surface fluxes by atmospheric convection in the TOGA COARE region. *Mon. Wea. Rev.,* **124,** 816–837.

Kalnay, E., and Coauthors, 1996: The NCEP/NCAR 40-Year Reanalysis Project. *Bull. Amer. Meteor. Soc.,* **77,** 437–472.

Kang, S., I. Held, D. Frierson, and M. Zhao, 2008: The response of the ITCZ to extratropical thermal forcing: Idealized slab-ocean experiments with a GCM. *J. Climate,* **21,** 3521–3532.

Khairoutdinov, M., and K. Emanuel, 2010: Aggregation of convection and the regulation of climate. Preprints, *29th Conf. on Hurricanes and Tropical Meteorology,* Tucson, AZ, Amer. Meteor. Soc., P2.69. [Available online at http://ams.confex.com/ams/pdfpapers/168418.pdf.]

Laing, A., and J. M. Fritsch, 1997: The global population of mesoscale convective complexes. *Quart. J. Roy. Meteor. Soc.,* **123,** 389–405.

Larson, K., D. Hartmann, and S. Klein, 1999: Role of clouds, water vapor, circulation, and boundary layer structure in the sensitivity of the tropical climate. *J. Climate,* **12,** 2359–2374.

Lau, K., H. Wu, and S. Bony, 1997: The role of large-scale atmospheric circulation in the relationship between tropical convection and sea surface temperature. *J. Climate,* **10,** 381–392.

Liebmann, B., and C. Smith, 1996: Description of a complete (interpolated) OLR dataset. *Bull. Amer. Meteor. Soc.,* **77,** 1275–1277.

Lin, J., and Coauthors, 2006: Tropical intraseasonal variability in 14 IPCC AR4 climate models. Part I: Convective signals. *J. Climate,* **19,** 2665–2690.

Liu, C., E. Zipser, and S. Nesbitt, 2007: Global distribution of tropical deep convection: Different perspectives from TRMM infrared and radar data. *J. Climate,* **20,** 489–503.

Madden, R., and P. Julian, 1994: Observations of the 40–50-day tropical oscillation: A review. *Mon. Wea. Rev.,* **122,** 814–837.

Mapes, B. E., 1993: Gregarious tropical convection. *J. Atmos. Sci.,* **50,** 2026–2037.

——, and R. Houze Jr., 1993: Cloud clusters and superclusters over the Oceanic Warm Pool. *Mon. Wea. Rev.,* **121,** 1398–1415.

——, and R. B. Neale, 2011: Parameterizing convective organization. *J. Adv. Model. Earth Syst.,* **3,** M06004, doi:10.1029/2011MS000042.

Moncrieff, M., 2004: Analytic representation of the large-scale organization of tropical convection. *J. Atmos. Sci.,* **61,** 1521–1538.

Nakazawa, T., 1988: Tropical super clusters within intraseasonal variations over the western Pacific. *J. Meteor. Soc. Japan,* **66,** 823–839.

Nolan, D., E. Rappin, and K. Emanuel, 2007: Tropical cyclogenesis sensitivity to environmental parameters in radiative–convective equilibrium. *Quart. J. Roy. Meteor. Soc.,* **133,** 2085–2107.

Pierrehumbert, R., 1995: Thermostats, radiator fins, and the local runaway greenhouse. *J. Atmos. Sci.,* **52,** 1784–1806.

Qian, L., G. Young, and W. Frank, 1998: A convective wake parameterization scheme for use in general circulation models. *Mon. Wea. Rev.,* **126,** 456–469.

Randall, D., Harshvardhan, D. Dazlich, and T. Corsetti, 1989: Interaction among radiation, convection, and large-scale dynamics in a general circulation model. *J. Atmos. Sci.,* **46,** 1943–1970.

Raymond, D., 1995: Regulation of moist convection over the west Pacific warm pool. *J. Atmos. Sci.,* **52,** 3945–3959.

Redelsperger, J.-L., 1997: The mesoscale organization of deep convection. *The Physics and Parameterization of Moist Atmospheric Convection,* R. K. Smith, Ed., Kluwer Academic, 59–98.

——, F. Guichard, and S. Mondon, 2000: A parameterization of mesoscale enhancement of surface fluxes for large-scale models. *J. Climate,* **13,** 402–421.

Roca, R., and V. Ramanathan, 2000: Scale dependence of monsoonal convective systems over the Indian Ocean. *J. Climate,* **13,** 1286–1298.

——, and Coauthors, 2010: On the water and energy cycle. *C. R. Geosci.,* **342,** 390–402, doi:10.1016/j.crte.2010.01.003.

——, R. Guzman, J. Lemond, L. Picon, and H. Brogniez, 2011: Free tropospheric humidity in the inter tropical belt. *Surv. Geophys.,* **24,** 555–574.

Saxen, T., and S. Rutledge, 1998: Surface fluxes and boundary layer recovery in TOGA COARE: Sensitivity to convective organization. *J. Atmos. Sci.,* **55,** 2763–2781.

Simmons, A. J., S. Uppala, D. Dee, and S. Kobayashi, 2007: ERA-Interim: New ECMWF reanalysis products from 1989 onwards. *ECMWF Newsletter,* No. 110, ECMWF, Reading, United Kingdom, 25–35.

Slingo, A., and J. Slingo, 1988: The response of a general circulation model to cloud longwave radiative forcing. I: Introduction and initial experiments. *Quart. J. Roy. Meteor. Soc.,* **114,** 1027–1062.

Spencer, R., and W. Braswell, 1997: How dry is the tropical free troposphere? Implications for global warming theory. *Bull. Amer. Meteor. Soc.,* **78,** 1097–1106.

Tompkins, A., 2001: Organization of tropical convection in low vertical wind shears: The role of water vapor. *J. Atmos. Sci.,* **58,** 529–545.

Winker, D., M. Vaughan, A. Omar, Y.-X. Hu, K. Powell, Z. Liu, W. Hunt, and S. Young, 2009: Overview of the CALIPSO mission and CALIOP data processing algorithms. *J. Atmos. Oceanic Technol.,* **26,** 2310–2323.

Yang, G., B. Hoskins, and J. Slingo, 2003: Convectively coupled equatorial waves: A new methodology for identifying wave structures in observational data. *J. Atmos. Sci.,* **60,** 1637–1654.

Young, G., S. Perugini, and C. Fairall, 1995: Convective wakes of the equatorial western Pacific during TOGA. *Mon. Wea. Rev.,* **123,** 110–123.

Yuan, J., and R. Houze Jr., 2010: Global variability of mesoscale convective system anvil structure from A-Train satellite data. *J. Climate,* **23,** 5864–5888.

Zurovac-Jevtic, D., S. Bony, and K. Emanuel, 2006: On the role of clouds and moisture in tropical waves: A two-dimensional model study. *J. Atmos. Sci.,* **63,** 2140–2155.